

## Damage assessment of a bridge based on mode shapes estimated by responses of passing vehicles

Yoshinobu Oshima<sup>\*1</sup>, Kyosuke Yamamoto<sup>2a</sup> and Kunitomo Sugiura<sup>1b</sup>

<sup>1</sup>Graduate School of Engineering, Kyoto University, Kyoto, 604-8530, Japan

<sup>2</sup>Graduate School of Systems and Information Engineering, University of Tsukuba, Tsukuba, Japan

(Received July 1, 2012, Revised August 15, 2013, Accepted August 22, 2013)

**Abstract.** In this study, an indirect approach is developed for assessing the state of a bridge on the basis of mode shapes estimated by the responses of passing vehicles. Two types of damages, i.e., immobilization of a support and decrease in beam stiffness at the center, are evaluated with varying degrees of road roughness and measurement noise. The assessment theory's feasibility is verified through numerical simulations of interactive vibration between a two-dimensional beam and passing vehicles modeled simply as sprung mass. It is determined that the damage state can be recognized by the estimated mode shapes when the beam incurs severe damage, such as immobilization of rotational support, and the responses contain no noise. However, the developed theory has low robustness against noise. Therefore, numerous measurements are needed for damage identification when the measurement is contaminated with noise.

**Keywords:** damage identification; bridge vibration; mode shape; bridge; vehicle interaction

---

### 1. Introduction

Modal parameters such as frequency and mode shape are important to the monitoring of bridge health because variations in these parameters may indicate bridge damage. Among these parameters, frequency is the most fundamental in terms of assessing bridge damage. Bridge frequencies can be identified from records of vibration directly obtained by sensors installed on the bridge; this method is hence referred to as a direct approach method. An excellent review of frequency identification by this direct approach was reported by Salawu and William (1995) and Salawu (1997). In addition, Doebling *et al.* (1996) presented a research summary on frequency-based damage detection. Time–frequency analysis has also been applied for bridge damage assessment to enhance the accuracy of assessment (Nguyen and Tran 2010). However, such direct approaches carry limitations regarding efficiency improvement. Although vibration data is collected by quick and easy methods such as the use of wireless sensors (Gangone *et al.* 2012), their installation requires one to spend time being physically present at the bridge, which is impractical considering the large number of bridges under evaluation. To maintain such a large

---

\*Corresponding author, Associate Professor, E-mail: [yoshinobu.oshima.3a@kyoto-u.ac.jp](mailto:yoshinobu.oshima.3a@kyoto-u.ac.jp)

<sup>a</sup> Assistant Professor, E-mail: [yama@ise.kuciv.kyoto-u.ac.jp](mailto:yama@ise.kuciv.kyoto-u.ac.jp)

<sup>b</sup> Professor, E-mail: [sugiura.kunitomo.4n@kyoto-u.ac.jp](mailto:sugiura.kunitomo.4n@kyoto-u.ac.jp)

number of bridges properly, more rapid, simpler and easier methods are needed even if the accuracy of assessment decreases. Such methods can be referred as a screening technique in which the bridges are roughly assessed to select the bridges having suspected damages. Such a technique can significantly reduce inspection time because the remaining structures can be evaluated in the next planned review.

To achieve this, an additional concept of an indirect approach to identify bridge frequency has recently been proposed by Yang *et al.* (2004). The basic concept of this approach involves extracting the natural frequency of the bridge from the dynamic responses of vehicles passing over it. Although natural frequency is not so sensitive to damage, this approach can be used for screening technique. Several studies have verified the basic concept of this approach both theoretically (Yang and Lin 2005, Yang and Chang 2009a, b, Siringoringo and Fujino 2012) and experimentally (Lin and Yang 2005). Several researchers have recently extended this approach to damage identification. Yin and Tang (2011) applied this technique to identify cable tension loss and deck damage in a cable-stayed bridge by utilizing principle component analysis on the vehicle responses to extract the index for these damages. Kim and Kawatani (2008) and Bu *et al.* (2006) proposed an algorithm to identify flexural stiffness reduction in beams on the basis of vehicle responses. In addition, the damping effect has been evaluated by using the responses of passing vehicles (McGetrick 2009, Gonzalez *et al.* 2012).

Among other modal parameters, mode shape is more preferable for damage detection because it is more sensitive to structural damage (Yong *et al.* 2002). Zhang *et al.* (2012) introduced the possibility of identifying mode shape information from vehicle responses by using a tapping device. They determined that a passing vehicle equipped with a sensor and a tapping system can induce several sinusoidal forces on the bridge mode shape, where by squares or operating deflection shape curvatures can be evaluated by the response of the vehicle (Zhang *et al.* 2013). However, this promising method requires specific tapping devices for enhancing bridge vibration.

Thus, this study aims to develop an indirect approach for assessing the state of a bridge on the basis of mode shape estimated by the responses of passing vehicles without a special device. Two types of damages are examined with varying degrees of road roughness and measurement noises. The assessment theory's feasibility is verified by numerical simulations of interactive vibration between a two-dimensional beam and passing vehicles modeled simply as sprung mass. This paper is organized into the following sections: Section 2 presents a theoretical explanation on the proposed method, Section 3 describes numerical verification, and Section 4 presents conclusions. In Section 3, an outline of numerical simulation is first described, and the appropriate number of vehicles is determined taking into consideration standard parameters of roughness, velocity, and mass. The effects of surface roughness, velocity, and vehicle mass are then discussed. Finally, the influence of noise on the estimation results is discussed, and a technique for eliminating the noise effect is presented.

## 2. Formulation of theory

### 2.1 Outline of theory

In our basic estimation theory, more than four monitoring vehicles and two heavy trucks are used, and the following indications are assumed:

- Monitoring vehicles move at a constant velocity; two heavy trucks are located before and after the monitoring vehicles at constant intervals in a convoy, as shown in Fig. 1.
- Heavy vehicles and monitoring vehicles are simplified as a sprung mass model.
- The bridge is modeled as a simple beam.
- Bridge displacement can be decomposed into uncorrelated generalized coordinates and orthogonal mode shape functions.

It should be noted that the heavy trucks are required for amplifying the bridge vibrations; however, their responses are not used in the estimation. Furthermore, although it is not necessary the distance and velocity of these trucks as constant, this assumption is nonetheless made for simplicity. With regard to the assumed convoy of vehicles, one example is such that cargos with one axle are towed by a heavy vehicle.

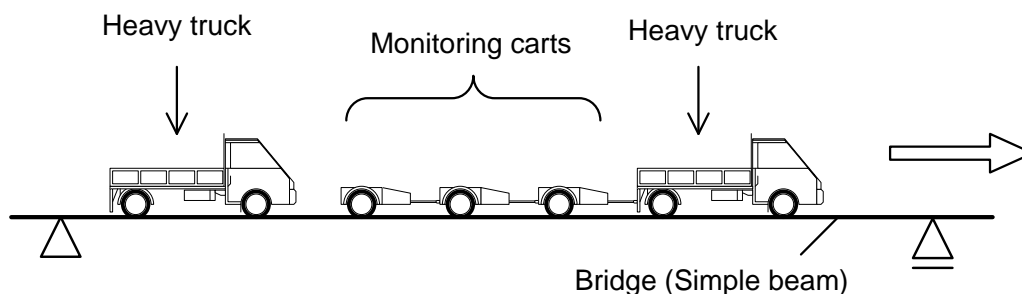


Fig. 1 Convoy of monitoring vehicles and heavy trucks passing over a bridge

The sequence of the estimation theory, consisting of four steps, is illustrated in Fig. 2. In general, a vehicle moving on the road with roughness vibrates due to the interaction between the road surface and vehicle's axle. The surface roughness can be regarded as a forced displacement applying to the axle. Especially on a bridge, the road surface varies due to the bridge displacement as well as the surface roughness itself. Thus, in the first step, forced displacement including road roughness and bridge displacement is estimated from the acceleration of sprung mass and the relative displacement between the mass and road surface. In the second step, bridge displacement is obtained by simply subtracting the forced displacement of one vehicle from that of another, both of which move exactly on the same path. In the third step, the obtained displacement is converted to that observed on a fixed location because the displacement in the second step is that observed from the moving vehicles, and thus the displacement is a function of the moving coordinate. For conversion from moving to fixed coordinates, mode shape is interpolated by using base functions such as polynomial functions. Finally, mode shape is estimated from the obtained deformations with a fixed coordinate by singular value decomposition of the converted deformations. Then, the obtained mode shapes are compared with base line mode shapes to evaluate the state of the bridge. When the initial results of the estimated mode shapes are determined, these shapes are utilized for base line, and the difference between the initial and current states can be identified by comparison with these mode shapes. If no information is available on the initial state, ideal mode shapes such as sine curves should be assumed for the base line. In the following sections, the estimation theory is described in detail.

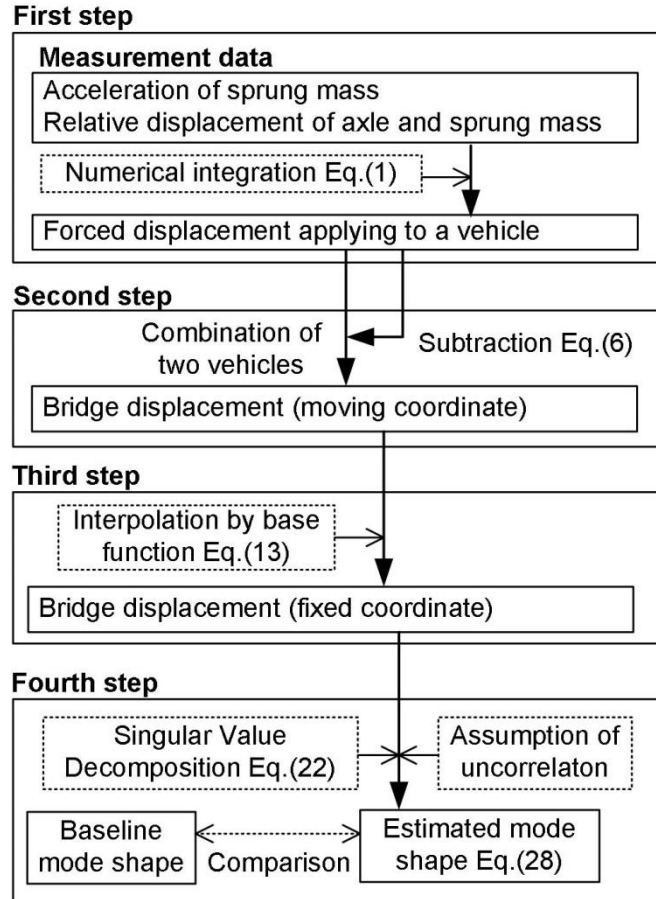


Fig. 2 Sequence of the four steps performed in our estimation

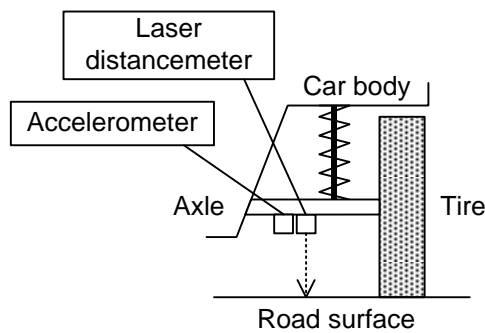


Fig. 3 Placement of laser distance meter and accelerometer on the vehicle axle

2.1 Step 1: estimation of forced displacement

To estimate the forced displacement applied to the vehicle system, the relative displacement between the vehicle body (or axle) and road surface and the acceleration of the body (or axle) are recorded at the same location. For example, relative displacement can be measured by a laser distance meter installed on an axle, as shown in Fig. 3, and acceleration is recorded by an accelerometer.

Let the forced displacement, relative displacement, and acceleration of a vehicle  $i$  ( $= 1, \dots, n_{ve}$ ) be  $u_i(t_k)$ ,  $\delta_i(t_k)$ , and  $\ddot{z}_i(t_k)$  ( $t_k = k\Delta t, k = 0, \dots, n_t$ ), respectively. Then, the vertical displacement of the vehicles  $z_i(t_k)$  and can be obtained by numerically integrating the acceleration as

$$z_i(t_k) = \sum_{i=0}^k (z_i(t_{k-1}) + \dot{z}_i(t_{k-1})\Delta t + \frac{1}{6}(2\ddot{z}_i(t_{k-1}) + \ddot{z}_i(t_k))\Delta t^2) \tag{1}$$

where

$$\dot{z}_i(t_k) = \sum_{i=0}^k \left( \dot{z}_i(t_{k-1}) + \frac{1}{2}(\ddot{z}_i(t_{k-1}) + \ddot{z}_i(t_k))\Delta t \right) \tag{2}$$

The forced displacement applied to vehicle  $i, u_i(t_k)$ , can be given as

$$u_i(t_k) = \delta_i(t_k) + z_i(t_k). \tag{3}$$

Note that the initial values for the system are assumed to be 0, which indicates that the vehicle is stopped at the moment of initial measurement.

2.2 Step 2: reduction of road roughness

To obtain bridge displacement, road roughness is subtracted from the forced displacement obtained in the first step. Now, let the location of vehicle  $i$  at the time of  $t_k$  be  $x = \tilde{x}_i(t_k)$  and the bridge deformation and road roughness along vehicle  $i$  be  $y(\tilde{x}_i, t_k) = \tilde{y}_i(t_k)$  and  $r(\tilde{x}_i) = \tilde{r}_i(t_k)$ , respectively, as shown in Fig. 4. Note that  $y(x, t)$  indicates the bridge displacement at position  $x$  and time  $t$ , and  $r(x)$  indicates the roughness at position  $x$ . Note also that  $\tilde{y}_i$  and  $\tilde{r}_i$  are functions of position  $\tilde{x}_i$  which is also a function of time; thus,  $t_k$  is explicitly described in these expressions. Then, the forced displacement of vehicle  $i$  can be given by

$$u_i(t_k) = \tilde{y}_i(t_k) - \tilde{r}_i(t_k) \tag{4}$$

When all vehicles move on the exact same path, the roughness contained in the forced displacement is identical for all vehicles at the same location, whereas bridge displacement differs, i.e.,

$$r_i(t_l) = r_{i+1}(t_{l+\tau}) \text{ or } \tilde{x}_i(t_l) = \tilde{x}_{i+1}(t_{l+\tau}) \tag{5}$$

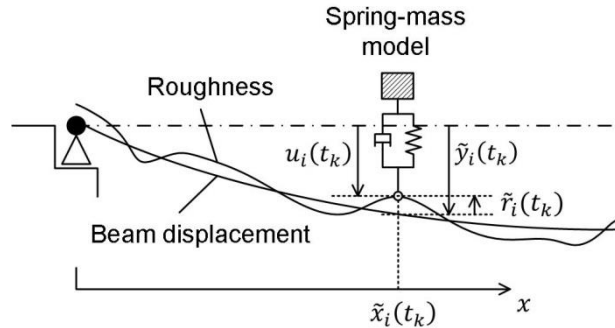


Fig. 4 Geometric relationship of beam displacement and roughness

Eq. (5) is drawn on the assumption that vehicle  $i$  is followed by vehicle  $i + 1$  with a time difference of  $\tau$ , and vehicle  $i$  and  $i + 1$  pass the same location at  $t = t_I$  and  $t = t_{I+\tau}$ , respectively. Thus, by simply subtracting the forced displacement of vehicle  $i$  from that of vehicle  $i + 1$ , roughness can be eliminated

$$\begin{aligned} u_i(t_I) - u_{i+1}(t_{I+\tau}) &= \tilde{y}_i(t_I) - \tilde{y}_{i+1}(t_{I+\tau}) \\ &= y(\tilde{x}_i, t_I) - y(\tilde{x}_{i+1}, t_{I+\tau}) \equiv \Delta\tilde{y}_i(t_I) \end{aligned} \quad (6)$$

where  $\Delta\tilde{y}_i(t_I)$  is the difference in bridge displacement at  $x = \tilde{x}_i(t_I)$ , which is a moving coordinate. The vehicle location  $\tilde{x}_i$  is then regarded as a locus of moving observation points; thus, the number of moving observation points becomes  $n_{mov}$ , i.e.,  $n_{ve} - 1$ . Hereafter,  $\tilde{x}_i$  ( $i = 1, \dots, n_{mov}$ ) indicates the moving observation point of  $\Delta\tilde{y}_i(t_k)$ . To reduce the accumulated errors in the double integral at the first step, the following boundary condition is considered: when vehicle  $i$  enters the bridge at  $t = t_0$  ( $x = 0$ ) and leaves the bridge at  $t = t_{n_L}$  ( $x = L$ )

$$\begin{aligned} \Delta\tilde{y}_i(t_0) &= u_i(t_0) - u_{i+1}(t_0 + \tau) = y(0, t_0) - y(0, t_0 + \tau) = 0 \\ \text{and } \Delta\tilde{y}_i(t_{n_L}) &= u_i(t_{n_L}) - u_{i+1}(t_{n_L} + \tau) = y(L, t_{n_L}) - y(L, t_{n_L} + \tau) = 0 \end{aligned} \quad (7)$$

are valid because the bridge displacements at  $x = 0$  and  $x = L$  are always 0. Thus, the accumulative errors at  $t = t_{n_L}$  due to the double integral are linearly redistributed to the value of  $\Delta\tilde{y}_i(t_k)$  from  $x = 0$  to  $x = L$ . The most difficult step is to synchronize all data obtained by an individual monitoring vehicle. However, synchronization is necessary because the roughness can be deleted at the exact same location, and the data should be strictly allocated to the position. For example, such information can be realized by counting the tire cycles to determine the exact distance from the start point.

### 2.3 Step 3: conversion from moving to fixed observation

Because the monitoring vehicle moves over the bridge, the deformation obtained in the second step is along the moving vehicle, which is a function of the moving coordinate. Thus, in this step, the obtained deformation,  $\Delta\tilde{y}_i(t_k)$ , is converted into that at the fixed position, so that it becomes the function of a fixed coordinate.

To convert the moving coordinate into a fixed one, we adopt the concept of modal superposition. The vertical deflection  $y(x, t)$  for a two-dimensional beam in a series form can be expressed as

$$y(x, t) = \sum_{l=1}^{n_d} \phi_l(x)q_l(t) \tag{8}$$

where  $q_k(t)$  and  $\phi_k(x)$  denote the generalized coordinate and shape function of the  $l$ th vibration mode, respectively, and  $n_d$  is the maximum degree of assumed modes. By using this expression, the differences of bridge displacement  $\Delta\tilde{y}_i(t_k)$  can be also obtained in the form

$$\Delta\tilde{y}_i(t_k) = \sum_{l=1}^{n_d} \phi_l(\tilde{x}_i(t_k)) \{q_l(t_k) - q_l(t_k + \tau)\} \tag{9}$$

Then, by assuming that the number of moving observation points  $n_{mov}(= n_{ve} - 1)$  is equal to  $n_d$ , the mode shape matrix, which is a function of time, can be given by

$$\Phi(t_k) = \begin{bmatrix} \phi_1(\tilde{x}_1(t_k)) & \cdots & \phi_{n_d}(\tilde{x}_1(t_k)) \\ \vdots & \ddots & \vdots \\ \phi_1(\tilde{x}_{n_d}(t_k)) & \cdots & \phi_{n_d}(\tilde{x}_{n_d}(t_k)) \end{bmatrix} \tag{10}$$

and the difference of generalized coordinates can be expressed in the form

$$\Delta\mathbf{q}(t_k) = \begin{Bmatrix} q_1(t_k) - q_1(t_k + \tau) \\ \vdots \\ q_{n_d}(t_k) - q_{n_d}(t_k + \tau) \end{Bmatrix} \tag{11}$$

Thus, the difference in bridge displacement obtained by  $n_{mov}$  moving observation points can be expressed by

$$\Delta\tilde{\mathbf{y}}(t_k) = \begin{Bmatrix} \Delta\tilde{y}_1(t_k) \\ \vdots \\ \Delta\tilde{y}_{n_d}(t_k) \end{Bmatrix} = \Phi(t_k)\Delta\mathbf{q}(t_k) \tag{12}$$

The above equation can be used instead of bridge displacement for mode estimation because this equation excludes roughness. Note that the number of observation points determines the maximum degree of mode shapes to be estimated.

Now let us assume fixed observation points at  $\hat{x}_j(j = 1, \dots, n_{fix})$ , as shown in Fig. 5, with constant intervals. Note that although fixed observations can be at any location, for simplicity, they are allocated equivalently in this study.

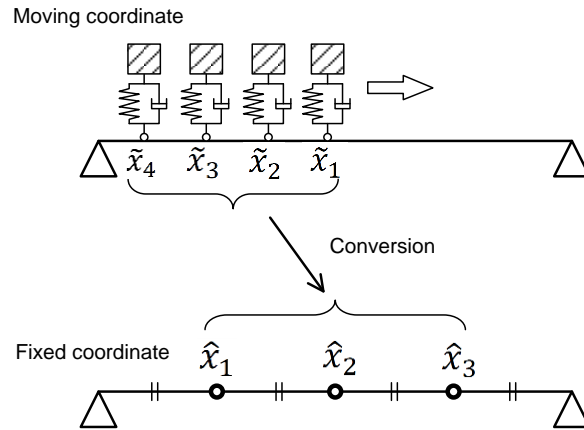


Fig. 5 Conversion from moving to fixed coordinates

Then let us also assume that  $\phi_l(x)$  is interpolated by  $n_d$  base functions,  $N_s(x)$ , as follows

$$\phi_l(x) = \sum_{s=1}^{n_d} a_{sl} N_s(x) \quad (13)$$

where  $a_{sl}$  is a constant coefficient with respect to  $N_s(x)$ , which is selected to satisfy the following conditions

$$N_s(\hat{x}_j) = \begin{cases} 1 & \dots (s = j) \\ 0 & \dots (s \neq j) \end{cases} \quad (14)$$

This equation indicates that the value of the  $j$ th base function becomes 1 at the fixed point for  $\hat{x}_j$  and 0 at other fixed points. Generally, several base functions can be used to satisfy the above equation. However, in this study, a Lagrange base function is adopted such as

$$N_s(x) = \prod_{\substack{l=1 \\ (l \neq s)}}^n \frac{x - \hat{x}_l}{\hat{x}_s - \hat{x}_l} \quad (15)$$

Other functions such as sinusoidal functions can be adopted for the base function, and the highest accuracy can be attained for the estimation of an ideal state. However, robustness against noise decreases dramatically when sinusoidal functions are used. The Lagrange function is adopted because the robustness against noise is higher than that in the other functions tested by the authors. With regard to Lagrange base function, it is obvious that fitting performance itself increases as the number of base functions increases. However, when the number of functions increases, the number of observation points also increases, which leads to ill-conditioning, as discussed subsequently. Thus, the proper number of functions, i.e., observation points, should be determined by considering the accuracy of mode shape estimation. Note that other adequate functions that can improve the estimation performance may exist, but these are not tested herein.

By substituting  $x = \hat{x}_j$  into Eq. (13), the following relationship can be obtained

$$\phi_l(\hat{x}_j) = \sum_{s=1}^n a_{sl} N_s(\hat{x}_j) = a_{jl} \tag{16}$$

This equation indicates that the coefficients of base functions are equal to the mode shapes that are to be estimated. Because the maximum degree of mode shapes is  $n_d$ , the number of fixed observation points,  $n_{fix}$ , should be equal to  $n_d$ .

On the other hand, from Eqs. (9), (13), and (16), the differences of bridge deformation at  $x = \tilde{x}_i(t_k)$  can be expressed as

$$\begin{aligned} \Delta \tilde{y}_i(t_k) &= \sum_{l=1}^n \phi_l(\tilde{x}_i(t_k)) \{q_l(t_k) - q_l(t_k + \tau)\} \\ &= \sum_{l=1}^n \sum_{s=1}^n \phi_l(\hat{x}_j) N_s(\tilde{x}_i(t_k)) \{q_l(t_k) - q_l(t_k + \tau)\} \end{aligned} \tag{17}$$

where  $j = 1, \dots, n_d$ . Thus, from Eqs. (12) and (17), the bridge deformation vector along the moving coordinates ( $x = \tilde{x}_1(t_k), \dots, \tilde{x}_n(t_k)$ ) can be given by

$$\Delta \tilde{\mathbf{y}}(t_k) = \mathbf{\Phi}(t_k) \Delta \mathbf{q}(t_k) = \mathbf{N}(t_k) \widehat{\mathbf{\Phi}} \Delta \mathbf{q}(t_k) \tag{18}$$

where  $\mathbf{N}(t_k)$  is defined by

$$\mathbf{N}(t_k) = \begin{bmatrix} N_1(\tilde{x}_1(t_k)) & \cdots & N_{n_d}(\tilde{x}_1(t_k)) \\ \vdots & \ddots & \vdots \\ N_1(\tilde{x}_{n_d}(t_k)) & \cdots & N_{n_d}(\tilde{x}_{n_d}(t_k)) \end{bmatrix} \tag{19}$$

and  $\widehat{\mathbf{\Phi}}$  is defined by

$$\widehat{\mathbf{\Phi}} = \begin{bmatrix} \phi_1(\hat{x}_1) & \cdots & \phi_{n_d}(\hat{x}_1) \\ \vdots & \ddots & \vdots \\ \phi_1(\hat{x}_{n_d}) & \cdots & \phi_{n_d}(\hat{x}_{n_d}) \end{bmatrix} \tag{20}$$

Then, by multiplying Eq. (18) by the inverse matrix  $\mathbf{N}(t_k)$  to the left, the following equation can be obtained

$$\begin{aligned} \mathbf{N}(t_k)^{-1} \Delta \tilde{\mathbf{y}}(t_k) &= \widehat{\mathbf{\Phi}} \Delta \mathbf{q}(t_k) = \left\{ \begin{array}{c} \sum_{l=1}^{n_d} \phi_l(\hat{x}_1) \{q_l(t_k) - q_l(t_k + \tau)\} \\ \vdots \\ \sum_{l=1}^{n_d} \phi_l(\hat{x}_{n_d}) \{q_l(t_k) - q_l(t_k + \tau)\} \end{array} \right\} \\ &= \left\{ \begin{array}{c} y(\hat{x}_1, t_k) - y(\hat{x}_1, t_k + \tau) \\ \vdots \\ y(\hat{x}_{n_d}, t_k) - y(\hat{x}_{n_d}, t_k + \tau) \end{array} \right\} \equiv \left\{ \begin{array}{c} \Delta \hat{y}_1(t_k) \\ \vdots \\ \Delta \hat{y}_{n_d}(t_k) \end{array} \right\} = \Delta \tilde{\mathbf{y}}(t_k) \end{aligned} \tag{21}$$

This equation indicates that the differences in bridge deformation at the fixed position  $\hat{x}_j$  and time  $t_k$ , i.e.,  $\Delta\hat{y}_i(t_k) = y(\hat{x}_j, t_k) - y(\hat{x}_j, t_k + \tau)$ , can be obtained by multiplying  $\Delta\tilde{\mathbf{y}}(t_k)$  by  $\mathbf{N}(t_k)^{-1}$  to the left. Note that  $\mathbf{N}(t_k)$  can be defined while the vehicles are in the section of  $[\hat{x}_1, \hat{x}_n]$ , as shown in Fig. 6, because interpolation by the Lagrange base function is defined in the node section  $[\hat{x}_1, \hat{x}_n]$ , and the boundary condition should be satisfied in this section. Both ends at the support location can be considered as observation points. To include these two points, dummy moving observation points, which are always 0, are added only into the first and last component of  $\Delta\tilde{\mathbf{y}}(t_k)$ . In this case, the entire span can be covered by interpolation, although the final accuracy of mode estimation is not significantly related to the interpolation of these end sections. Moreover, the estimation accuracy is nearly identical to the case that considers two points, even without considering the end sections. With regard to the time section, let  $t_a (= a\Delta t)$  be the time at which the last vehicle reaches  $\hat{x}_1$ , and let  $t_b (= b\Delta t)$  be the time at which the second vehicle reaches  $\hat{x}_n$ . Then, the total number of data for analysis becomes  $b - a + 1 (\equiv m)$ .

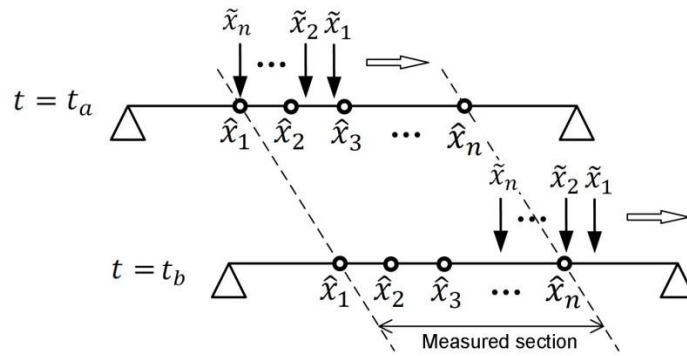


Fig. 6 Definition of measured section

#### 2.4 Step 4: estimation of mode shape and its evaluation

In this step, mode shape is estimated on the basis of the converted deformation of the bridge. Using the obtained deformation of  $\Delta\hat{\mathbf{y}}(t_k) = \mathbf{N}(t_k)^{-1}\Delta\tilde{\mathbf{y}}(t_k)$  ( $k = a, \dots, b$ ), let the matrix,  $\mathbf{D}$ , be given by

$$\mathbf{D} = [\Delta\hat{\mathbf{y}}(t_a) \quad \dots \quad \Delta\hat{\mathbf{y}}(t_b)] = [\mathbf{N}(t_a)^{-1}\Delta\tilde{\mathbf{y}}(t_a) \quad \dots \quad \mathbf{N}(t_b)^{-1}\Delta\tilde{\mathbf{y}}(t_b)] \quad (22)$$

The matrix  $\mathbf{D} \in \mathbb{R}^{na \times m}$  can be decomposed by singular value decomposition as

$$\mathbf{D} = \mathbf{U}\mathbf{\Sigma}\mathbf{V}^T \quad (23)$$

where  $\mathbf{U} \in \mathbb{R}^{na \times na}$  and  $\mathbf{V} \in \mathbb{R}^{m \times m}$  are orthogonal matrices and  $\mathbf{\Sigma} \in \mathbb{R}^{na \times m}$  is given by

$$\mathbf{\Sigma} = \begin{bmatrix} \Sigma_1 & & 0 & 0 & \cdots & 0 \\ & \ddots & & \vdots & & \vdots \\ 0 & & \Sigma_{n_d} & 0 & \cdots & 0 \end{bmatrix} = [\mathbf{\Sigma}_R \quad \mathbf{0}] \tag{24}$$

where  $\mathbf{\Sigma}_R \in R^{n_d \times n_d}$  is a matrix comprising  $n_d$  columns of  $\mathbf{\Sigma}$ , and  $\Sigma_1, \dots, \Sigma_{n_d}$  are singular values in descending order. Then,  $\mathbf{U}$  is normalized so that the maximum values of the element in each column are determined as

$$\bar{\mathbf{\Phi}} = \mathbf{U}\mathbf{S}^{-1} \tag{25}$$

where  $\mathbf{S} \in R^{n_d \times n_d}$  is the orthogonal matrix with the maximum values of each column of  $\mathbf{U}$  as an orthogonal element, and  $\bar{\mathbf{\Phi}}$  is the normalized matrix of  $\mathbf{U}$ . Now, if  $\mathbf{V}_R \in R^{m \times n_d}$  is defined as the matrix consisting of  $n_d$  columns of  $\mathbf{V}$ , Eq. (22) can be expanded as

$$\mathbf{D} = \mathbf{U}\mathbf{\Sigma}\mathbf{V}^T = \mathbf{U}\mathbf{\Sigma}_R\mathbf{V}_R^T = \bar{\mathbf{\Phi}}\mathbf{S}\mathbf{\Sigma}_R\mathbf{V}_R^T = \bar{\mathbf{\Phi}}\mathbf{\Delta}\bar{\mathbf{Q}} \tag{26}$$

where

$$\mathbf{\Delta}\bar{\mathbf{Q}} = \mathbf{S}\mathbf{\Sigma}_R\mathbf{V}_R^T \equiv [\mathbf{\Delta}\bar{\mathbf{q}}(t_a) \quad \cdots \quad \mathbf{\Delta}\bar{\mathbf{q}}(t_b)] \tag{27}$$

On the other hand,  $\mathbf{D}$  can be expressed directly by Eq. (21) in the form

$$\mathbf{D} = [\mathbf{\Delta}\hat{\mathbf{y}}(t_a) \quad \cdots \quad \mathbf{\Delta}\hat{\mathbf{y}}(t_b)] = [\hat{\mathbf{\Phi}}\mathbf{\Delta}\mathbf{q}(t_a) \quad \cdots \quad \hat{\mathbf{\Phi}}\mathbf{\Delta}\mathbf{q}(t_b)] = \hat{\mathbf{\Phi}}\mathbf{\Delta}\mathbf{Q} \tag{28}$$

where  $\mathbf{\Delta}\mathbf{Q} \equiv [\mathbf{\Delta}\mathbf{q}(t_a) \quad \cdots \quad \mathbf{\Delta}\mathbf{q}(t_b)]$ . Thus, from Eqs. (27) and (25), when the generalized coordinates are uncorrelated and the mode shape functions are orthogonal, the mode shape matrix  $\hat{\mathbf{\Phi}}$  corresponds to  $\bar{\mathbf{\Phi}}$ , and the generalized coordinate  $\mathbf{\Delta}\mathbf{q}(t_k)$  corresponds to  $\mathbf{\Delta}\bar{\mathbf{q}}(t_k)$ . Thus, if the above assumption is valid, the matrix of  $\bar{\mathbf{\Phi}}$  can be regarded as the mode shape matrix.

Finally, the state of the bridge is evaluated by comparing base line mode shapes with those estimated by the above theory on the basis of the averaged mode assurance criterion (MAC) values given by

$$\overline{\text{MAC}} = \frac{1}{n_d} \sum_{l=1}^{n_d} \frac{\left(\sum_{j=1}^{n_d} \bar{\phi}_l(\hat{x}_j)\varphi_l(\hat{x}_j)\right)^2}{\left(\sum_{j=1}^{n_d} \bar{\phi}_l^2(\hat{x}_j)\right)\left(\sum_{j=1}^{n_d} \varphi_l^2(\hat{x}_j)\right)} \tag{29}$$

where  $\varphi_l(\hat{x}_j)$  is the  $l$ th order of the base line mode shape at  $\hat{x}_j$ , and  $\bar{\phi}_l(\hat{x}_j)$  is the  $l$ th order of mode shape obtained by the proposed theory defined as the component of matrix,  $\bar{\mathbf{\Phi}}$ , in the form

$$\bar{\mathbf{\Phi}} = \begin{bmatrix} \bar{\phi}_1(\hat{x}_1) & \cdots & \bar{\phi}_{n_d}(\hat{x}_1) \\ \vdots & \ddots & \vdots \\ \bar{\phi}_1(\hat{x}_{n_d}) & \cdots & \bar{\phi}_{n_d}(\hat{x}_{n_d}) \end{bmatrix} \tag{30}$$

Note that although this theory is formulated in a two-dimensional beam, the theory can be extended to a three-dimensional beam by considering shear rotation,  $\gamma(x, t)$ , expressed by

$$\gamma_s(x, t) = \sum_l v_l(x) p_l(t) \tag{31}$$

where  $v_l$  is a shape function for shear mode, and  $p_l$  is a generalized coordinate for  $i$ th shear mode. On the basis of this model, shape function for rotation can also be approximated by base functions in the same manner as that for vertical displacement. Then, shear rotation and vertical displacement are obtained independently. In this case, monitoring vehicles should be located three-dimensionally to interpolate the horizontal curves of mode shapes.

### 3. Numerical verification

#### 3.1 Verification outline

Numerical simulation was conducted to verify the proposed theory. In this simulation, the vehicles and bridge were assumed to be a mass–spring system and a simple beam consisting of two-dimensional finite elements, respectively. In particular, monitoring vehicles were regarded as single-axle models and heavy trucks as double-axle models (Fig. 7). Bridge displacement, which is expressed by modal superposition with the maximum degree of  $m_s$ , can be discretized into  $n_s$  nodes ( $x = x_1, \dots, x_{n_s}$ ) in the form

$$\mathbf{y}(t) = \mathbf{X}\mathbf{q}(t) \tag{32}$$

where  $\mathbf{y}(t) = \{y(x_1, t), \dots, y(x_{n_s}, t)\}^T$  is the bridge displacement vector,  $\mathbf{q}(t) = \{q_1(t), \dots, q_{m_s}(t)\}^T$  is the general coordinates vector, and  $\mathbf{X} \in \mathbf{R}^{n_s \times m_s}$  is the mode shape matrix given by

$$\mathbf{X} = \begin{bmatrix} \phi_1(x_1) & \cdots & \phi_{m_s}(x_1) \\ \vdots & \ddots & \vdots \\ \phi_1(x_{n_s}) & \cdots & \phi_{m_s}(x_{n_s}) \end{bmatrix} \tag{33}$$

Note that mode shape matrix is obtained in advance by eigenvalue analysis for the non-damping system of the assumed beam.

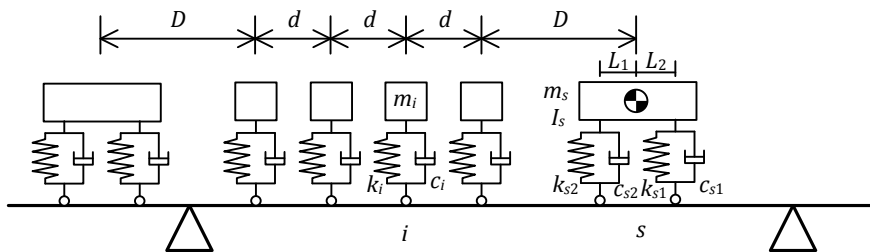


Fig. 7 Assumed model for verification

When total  $n_x$  contact forces of  $\mathbf{P}(t) = \{P_1(t), \dots, P_{n_x}(t)\}^T$  including single- and double-axle vehicles are acting on the bridge, the equation of motion of the bridge can be expressed by a discrete model as

$$\mathbf{M}_X \ddot{\mathbf{q}}(t) + \mathbf{C}_X \dot{\mathbf{q}}(t) + \mathbf{K}_X \mathbf{q}(t) = \mathbf{X}^T \mathbf{L}(t) \mathbf{P}(t) \tag{34}$$

where  $\mathbf{M}_X = \mathbf{X}^T \mathbf{M}_B \mathbf{X}$ ,  $\mathbf{C}_X = \mathbf{X}^T \mathbf{C}_B \mathbf{X}$ , and  $\mathbf{K}_X = \mathbf{X}^T \mathbf{K}_B \mathbf{X}$  are normalized modal mass, damping, and stiffness matrices, respectively, and  $\mathbf{L}(t) \in \mathbf{R}^{n_s \times n_x}$  is a transformation matrix. Note that  $\mathbf{M}_B \in \mathbf{R}^{n_s \times n_s}$ ,  $\mathbf{C}_B \in \mathbf{R}^{n_s \times n_s}$ , and  $\mathbf{K}_B \in \mathbf{R}^{n_s \times n_s}$  are diagonal matrices with the components  $M_i$ ,  $C_i$ , and  $K_i$  at the  $i$ th element, respectively.

On the other hand, the equation of motion of moving vehicles can be given by

$$\mathbf{M}_V \ddot{\mathbf{z}}(t) + \mathbf{C}_V \dot{\mathbf{z}}(t) + \mathbf{K}_V \mathbf{z}(t) = \mathbf{C}_V \dot{\mathbf{u}}(t) + \mathbf{K}_V \mathbf{u}(t) \tag{35}$$

where  $\mathbf{M}_V \in \mathbf{R}^{n_x \times n_x}$ ,  $\mathbf{C}_V \in \mathbf{R}^{n_x \times n_x}$ , and  $\mathbf{K}_V \in \mathbf{R}^{n_x \times n_x}$  are the mass, damping, and spring stiffness matrices of the vehicles, and  $\mathbf{z}(t) = \{z_1(t), \dots, z_{n_x}(t)\}^T$  and  $\mathbf{u}(t) = \{u_1(t), \dots, u_{n_x}(t)\}^T$  are vehicle responses and forced displacement, respectively. The details of the matrix are described in Table 1 (Ihsan *et al.* 2009).

Table 1 Matrix for double-axle model

Mass	Damping	Stiffness
$\begin{bmatrix} \frac{L_2 m_s}{L_1 + L_2} & \frac{L_1 m_s}{L_1 + L_2} \\ \frac{I_s}{L_1 + L_2} & -\frac{I_s}{L_1 + L_2} \end{bmatrix}$	$\begin{bmatrix} c_1 & c_2 \\ L_1 c_1 & -L_1 c_2 \end{bmatrix}$	$\begin{bmatrix} k_1 & k_2 \\ L_1 k_1 & -L_1 k_2 \end{bmatrix}$

\* $I_s$  is inertia moment

Then, by using transformation matrix  $\mathbf{L}(t)$  and roughness vector  $\mathbf{r}(t) = \{r_1(t), \dots, r_{n_x}(t)\}^T$ , forced displacement can be expressed by

$$\mathbf{u}(t) = \mathbf{L}^T(t) \mathbf{X} \mathbf{q}(t) + \mathbf{r}(t) \tag{36}$$

and the contact force of  $\mathbf{P}(t)$  can be expressed by

$$\mathbf{P}(t) = \mathbf{M}_P (\mathbf{g} - \ddot{\mathbf{z}}(t)) \tag{37}$$

where  $\mathbf{M}_P \in \mathbf{R}^{n_x \times n_x}$  is a mass matrix of vehicles for contact force, and  $\mathbf{g}$  and  $\ddot{\mathbf{z}}(t)$  are the vectors of gravity acceleration and acceleration responses of the vehicle, respectively. Note that  $\mathbf{M}_P$  is common to  $\mathbf{M}_V$  in the part of the matrix regarding the single-axle model, but the part regarding the double-axle model is diagonal and has components of  $\frac{L_2 m_s}{L_1 + L_2}$  and  $\frac{L_1 m_s}{L_1 + L_2}$  for the first and second axles, respectively.

Thus, to simulate bridge-vehicle vibration, the following equation of motion was solved by the Newmark- $\beta$  method with time increments of 1/1000 s,  $\beta = 1/6$ , and  $\gamma = 1/2$

$$\begin{aligned}
& \begin{bmatrix} \mathbf{M}_X & \mathbf{X}^T \mathbf{L}(t) \mathbf{M}_P \\ \mathbf{0} & \mathbf{M}_V \end{bmatrix} \begin{Bmatrix} \ddot{\mathbf{q}}(t) \\ \ddot{\mathbf{z}}(t) \end{Bmatrix} + \begin{bmatrix} \mathbf{C}_X & \mathbf{0} \\ -\mathbf{C}_V \mathbf{L}^T(t) \mathbf{X} & \mathbf{C}_V \end{bmatrix} \begin{Bmatrix} \dot{\mathbf{q}}(t) \\ \dot{\mathbf{z}}(t) \end{Bmatrix} \\
& + \begin{bmatrix} \mathbf{K}_X & \mathbf{0} \\ -\mathbf{K}_V \mathbf{L}^T(t) & \mathbf{K}_V \end{bmatrix} \begin{Bmatrix} \mathbf{q}(t) \\ \mathbf{z}(t) \end{Bmatrix} \\
& = \begin{Bmatrix} \mathbf{X}^T \mathbf{L}(t) \mathbf{M}_P \mathbf{g} \\ \mathbf{C}_V \dot{\mathbf{r}}(t) + \mathbf{K}_V \mathbf{r}(t) \end{Bmatrix}.
\end{aligned} \tag{38}$$

Here, the number of beam elements is 300 with lengths of 0.1 m, and the first to fifth modes are considered in the simulation. Vehicle parameters and bridge properties are assumed as stated in Tables 2 and 3, respectively. Note that the first eigenfrequency of the assumed bridge is 3.96 Hz, and that of the measuring vehicle is 1Hz, as determined by previous research (Lin and Yang 2005). In the estimation theory, four to six monitoring vehicles at 1-m intervals were considered. The shorter distance was preferable for interpolation. However, the inverse of the matrix  $\mathbf{N}$  became ill posed as the distance decreased; the shorter interval led to a significant decrease in estimation accuracy. Thus, the above condition was adopted for damage evaluation.

Road roughness was also given in the Monte Carlo simulation on the basis of the following power spectrum (Okabayashi 1979)

$$S_p = \frac{\alpha}{\Omega^\xi + \eta^\xi}, \tag{39}$$

where  $\Omega(\text{m}^{-1})$  is the surface frequency (the number of peaks per meter), and  $\alpha, \eta$ , and  $\xi$  are parameters determining surface conditions. As shown in Fig. 8, three grades of roughness were assumed by following ISO criteria, and three different roughness types were simulated for each grade. The surfaces of EG1 to EG3 correspond to “extra good,” the surfaces of GD1 and GD3 correspond to “good,” and the surfaces of ST1 and ST3 correspond to “standard,” according to ISO standards (Kawatani *et al.* 1997). The parameters used in this simulation are also listed in Table 4.

Table 2 Properties of vehicles assumed in the simulation

Heavy vehicle			
Mass	(kg)	$m_s$	10000
Damping	(kg/s)	$c_{s1}, c_{s2}$	74000
Spring Stiffness	(kg/s <sup>2</sup> )	$k_{s1}, k_{s2}$	760000
Inertia		$I$	90000
Length	(m)	$L_1, L_2$	3.0
Measuring vehicles			
Number		$N_{ve}$	4
Mass	(kg)	$m_i$	100
Damping	(kg/s)	$c_i$	50
Spring Stiffness	(kg/s <sup>2</sup> )	$k_i$	3950
Natural Frequency	(Hz)	$f_v = \sqrt{k_i/m_i}/2\pi$	1.00
Damping Coefficient		$\xi_v = 2c_i\sqrt{m_i k_i}$	0.30
Interval Distance	(m)	$d$	1.0
Common			
Run Speed	(m/s)	$v$	10.0
Distance	(m)	$D$	5.5

Table 3 Bridge properties assumed in the simulation

Physical parameters		
Length (m) $L$	Mass per Length (kg/m) $\rho A$	Flexural Stiffness (Nm) $EI$
30.0	3000	$1.56 \times 10^{10}$

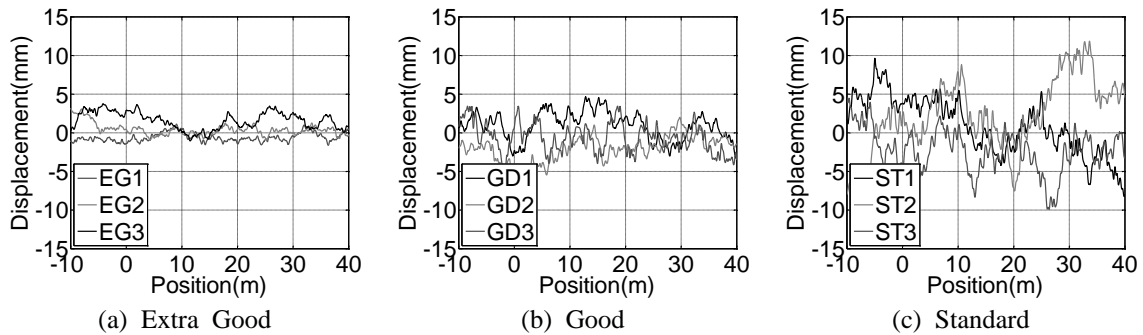


Fig. 8 Assumed model for verification

Table 4 Assumed parameters for road roughness types.

Name	ISO standard	$a$	$b$	$\xi$
EG1, EG2, EG3	Extra Good	0.001	0.05	2.00
GD1, GD2, GD3	Good	0.003	0.02	2.50
ST1, ST2, ST3	Standard	0.0098	0.08	1.92

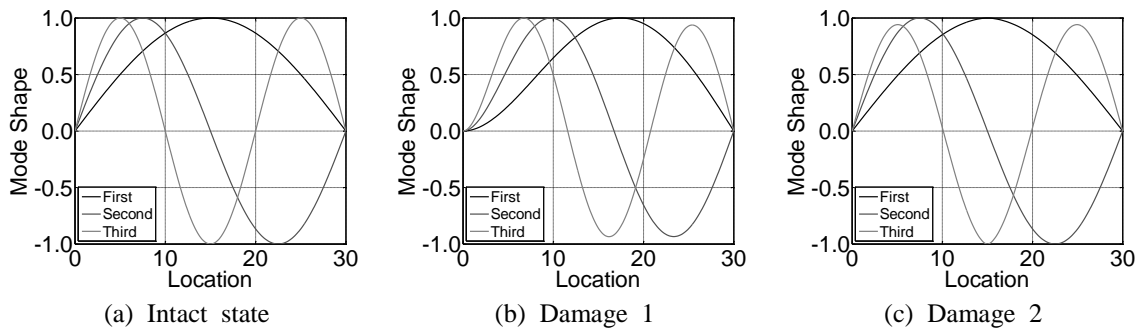


Fig. 9 Mode shapes of intact and damage states

Two different types of damage were assumed. For damage 1, one of two supports was fixed in rotation, representing a loss of rotational function of support; for damage 2, the stiffness of the beam at the center decreased by 40% with a length of 1 m. The mode shape of damage 1 differed from that of the intact state; however, the mode shape of damage 2 was nearly identical to that of the intact state, as shown in Fig. 9. The velocity of the vehicles also varied from 5 m/s to 15 m/s, and two different masses of heavy vehicles were also assumed. White noises of 1%, 3%, and 5% measurement of standard deviation were added into the measurement values in the first step.

### 3.2 Estimation results and discussion

#### 3.2.1 Effect of vehicle number

Fig. 10 shows the estimated results of mode shapes considering four, five, and six monitoring vehicles, each at a speed of 10m/s, over an intact beam with a surface of GD1. The noise effect is not considered. Note that the number of observation points and the maximum degree of modes to be estimated are determined according to the number of monitoring vehicles. For example, when the number of monitoring vehicles is four, three fixed observation positions are assumed, indicating that the mode shape is also estimated by only three given points.

As indicated in Fig. 10, the estimation accuracy of mode shape itself decreases as the number of vehicles increases, which may be attributed to ill-conditioning of the inverse matrix,  $\mathbf{N}(t_k)^{-1}$ , used in Step 3. If the matrix is illposed, a small error in calculation becomes significant in the final solution. Such ill-conditioning becomes critical as the number of vehicles increases or the intervals of vehicles decrease. To represent the accuracy of the result in a numerical calculation of matrix inversion, the condition number can be given by

$$\kappa(\mathbf{A}) = \frac{\sigma_{\max}(\mathbf{A})}{\sigma_{\min}(\mathbf{A})} \quad (40)$$

where  $\kappa(\mathbf{A})$  is the condition number of matrix  $\mathbf{A}$ , and  $\sigma_{\max}(\mathbf{A})$  and  $\sigma_{\min}(\mathbf{A})$  are the maximum and minimum of the singular value of  $\mathbf{A}$ , respectively (Pyzara *et al.* 2011). Fig. 11(a) shows the relationship between the condition number and the number of vehicles. From this figure, it is evident that the condition number decreases as the number of vehicle increases. This result indicates that an increase in the number of vehicles may lead to a decrease in accuracy. However, from the perspective of mode shape construction, additional nodes (i.e., additional vehicles) are preferable. Thus, vehicle number should be determined so that the effect of ill-conditioning is balanced with the enhancement of accuracy by increasing nodes in mode shapes.

Fig. 11(b) shows the averaged MAC in the intact and damage cases in which four, five, and six vehicles are used for estimation. From this figure, the averaged MAC decreases as the number of vehicles increases in any case. For any number of vehicles, the averaged MAC values in the intact and damage-2 cases are nearly identical; however, those in the damage-1 case are smaller than those in the other cases. The small value of MAC in the damage-1 case is attributed to the significant difference between the real mode shapes in the damage-1 case and those in the intact case; in other words, the MAC values based on sine functions for the estimated shapes become small. Because the averaged MAC values of exact solution for damage-1 and damage-2 cases are 0.9379 and 0.9999, respectively, the value estimated by using four vehicles is closer to the exact solution than those by the other vehicles. Thus, in this study, the number of monitoring vehicles is set to four.

Fig. 11(c) shows the MAC values corresponding to each degree of mode in the intact and damage cases using four vehicles. In the first mode, the MAC values for all cases are closer to 1.0 than those in the other modes. For the second and third modes, the MAC values in the damage-1 case are lower than those in the damage-2 and intact cases. Thus, to recognize the differences in these states, the MAC value of the second and third modes should be used for damage evaluation. However, this relationship may vary when the other profile and velocity are considered. Thus, the averaged MAC value can be appropriate for the index of damage evaluation.

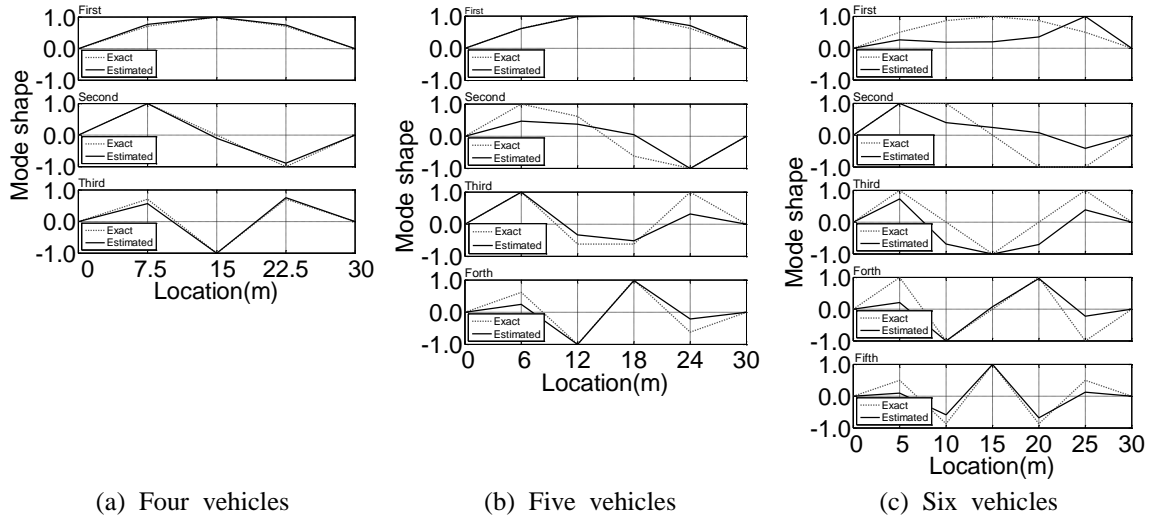


Fig. 10 Estimated mode shapes in cases of four, five, and six vehicles

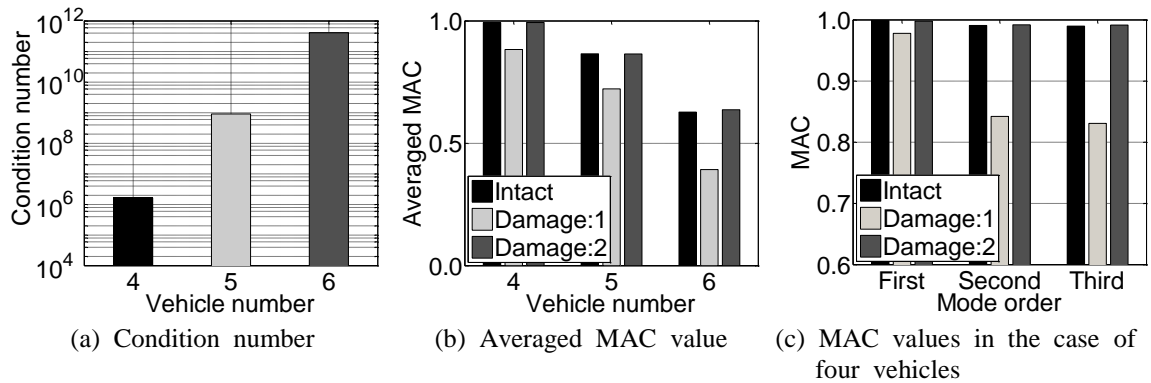


Fig. 11 Mode shapes of intact and damage states

3.2.2 Effects of surface roughness, vehicle velocity, and vehicle mass

In this section, the effects of surface roughness and the velocity and mass of the vehicles are discussed. In the fourth step of our theory, singular value decomposition is applied to the converted responses of the bridge with the assumption that the generalized coordinate of each mode is not correlated and mode shape vectors are orthogonal. Therefore, the performance of decomposition strongly depends on the correlation of actual generalized coordinates, which may vary with the conditions of roughness, as well as with vehicle velocity and mass. Thus, the MAC values of several cases are subsequently discussed from the perspective of correlation of the generalized coordinates.

The averaged MAC values of nine roughness types including three grades in the intact and damage-1 cases are plotted in Fig. 12(a) with respect to the correlation of the modes of the

generalized coordinates. In this figure, the degree of correlation is evaluated by

$$F(\mathbf{x}, \mathbf{y}) = \sum_i \log(x_i y_i) - \log|\det \mathbf{M}| \quad (41)$$

where  $F(\mathbf{x}, \mathbf{y})$  is the degree of correlations of  $\mathbf{x}(=x_1, \dots, x_n)$  and  $\mathbf{y}(=y_1, \dots, y_n)$ , and  $\mathbf{M}$  is a matrix with the component  $x_i y_j$  in the  $i$ th row and  $j$ th column. This equation represents the diagonal degree of  $\mathbf{M}$  (Kawamoto *et al.* 1997). This function is always larger than zero or equal to zero when  $\mathbf{M}$  is a diagonal matrix. Moreover, the function becomes infinity when every component of the matrix is identical. The matrix is a covariance matrix of  $\mathbf{x}$  and  $\mathbf{y}$ , and these two series vectors are completely uncorrelated; thus, the matrix becomes diagonal. This equation also denotes the degree of correlation between  $\mathbf{x}$  and  $\mathbf{y}$ . As indicated in the figure, in both cases of intact and damage, the correlation strengthens as the grade of roughness increases, which may be attributed to the fact that rough profiles generally exhibit lower correlation owing to the randomness of the profiles. Moreover, the MAC value decreases as the correlation increases. This tendency can be confirmed much more clearly in the damage-1 case than in the intact case. In general, the MAC values of the intact case are larger than those in the damage-1 case. The MAC values on the basis of sine functions may decrease when the mode shape to be estimated changes from the intact mode shape. Moreover, the accuracy of mode estimation partly depends on the performance of curve fitting by the Lagrange base function in the third step. Simple and symmetric shapes can generally be fitted with small errors by the base function. The difference between the MAC values of the two states may be attributed to these two factors. Thus, the difference between the bridge states in the intact and damage-1 cases can be recognized by the proposed method.

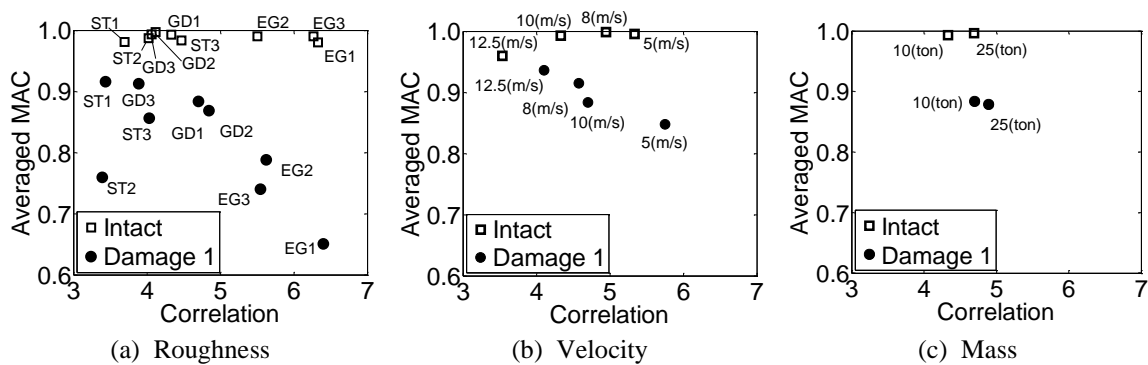


Fig. 12 Relationship between averaged MAC value and correlation of the generalized coordinates

Fig. 12(b) shows the relationship between the correlation and MAC values with different velocities in the intact and damage-1 cases. As confirmed above, it is also evident in this figure that the MAC value generally decreases as the correlation increases and that the MAC values in the intact cases are larger than those in the damage-1 case. In addition, the correlation essentially increases as velocity decreases partly because higher velocity vehicle may yield more randomness of bridge vibration. Fig. 12(c) also shows the relationship between the correlation and MAC values with different weights in the intact and damage cases. From this figure, the same tendency can be confirmed for different weights. In addition, the vehicle weight increases with the correlation. This

result may be attributed to the fact that light vehicles equally excite much higher components of bridge vibration.

Therefore, when four monitoring vehicles at 1-m intervals pass over a bridge and yield the converted bridge responses by our theory without noise, the state of the bridge can be recognized by the averaged MAC values.

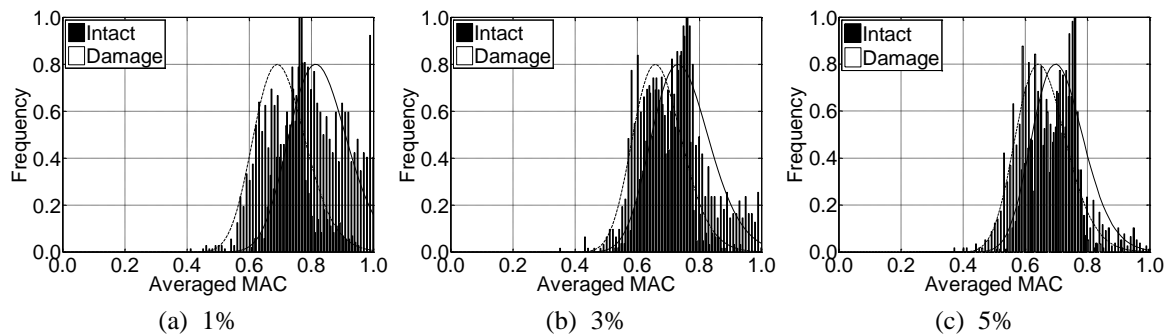


Fig. 13 Occurrence frequency of MAC values with 1%, 3%, and 5% noise

### 3.2.3 Effect of noise

The above analysis was conducted on the assumption that the responses were obtained without noise. To evaluate the effect of noise, we assumed that four monitoring vehicles at a velocity of 10 m/s pass over an intact and a damaged beam, each having the surface of GD1. Because the responses with random noise can be regarded as stochastic processes and the estimated MAC values strongly depend on the noise characteristics, 1000 measurement data with 1%, 3%, and 5% noise with respect to the standard deviation of the responses were produced. All measurement data were produced by adding different random noise with a given percent to a fixed measurement dataset without noise that delivered MAC of 0.999. Fig. 13 shows the occurrence histogram of averaged MAC in the cases with 1%, 3%, and 5% noise. In this figure, the data were fitted by lognormal distributions. The MAC values were widely distributed even for the intact and damage states, and the difference between these states decreased as noise increased. Even if the measurement data contained same amplitudes of noise, the obtained MAC values differed widely.

A decrease in the MAC value due to noise may be caused by a violation of the assumption in mode decomposition, which is sensitive to the correlation and orthogonality of the measurement data. If the noises have same amplitude but different phases, the nature of the signals differed from the perspective of decomposition and the MAC values obtained were different. Thus, the dispersion due to noise is much larger than the difference between the intact and damage states, and the proposed theory is not robust against noise. However, despite the dispersion of the MAC values, the mean values of the two distributions clearly differed in the case of 1% noise: the mean values of the intact and damage states were 0.83 and 0.70, respectively. In the case of 1% noise, 16 measurements were required to recognize the difference of 0.05 in the mean value of MAC with a significance level of 95%. The merit of our theory is its ease and rapidity of measurement: 16 measurements can be accommodated. However, in the case of 3% noise, 287 measurements are needed to recognize the difference of 0.01; for 5% noise, 755 measurements are needed to obtain a

difference of 0.005. These numbers are not appropriate for practical application; thus, robustness against noise should be improved.

#### 4. Conclusions

To identify the damage state of a bridge such as immobilization of rotational support, bridge mode shapes estimated by vehicle responses were evaluated. The feasibility of the identification theory was verified by numerical simulation of interactive vibration between a two-dimensional beam and passing vehicles modeled simply as sprung mass. Different mode shapes corresponding to different levels of damage with several degrees of road roughness and measurement noise were examined. As a result, it was determined that in the cases without noise, the averaged MAC values estimated by passing vehicles clearly differed between the intact and damage states with immobilization of rotational support. However, the proposed theory does not have robustness against noise, and numerous measurements are needed to recognize the differences between these states.

#### Acknowledgments

The authors gratefully acknowledge the support of this research by the Japan Society for the Promotion of Science (JSPS) under Grant-in-Aid for Young Scientists (A) 22686043.

#### References

- Bu, J.Q., Law, S.S. and Zhu, X.Q. (2006), "Innovative bridge condition assessment from dynamic response of a passing vehicle", *J. Eng. Mech. - ASCE*, **132**(12), 1372-1379.
- Doebeling, S.W., Farrar, C.R., Prime, M.B. and Shevitz, D.W. (1996), *Damage identification and health monitoring of structural and mechanical systems from changes in their vibration characteristics: a literature review*, Research Report No. LA-13070-MS, ESA-EA, Los Alamos National Laboratory, NM.
- Gangone, M.V., Whelan, M.J. and Janoyan, K.D. (2012), "Deployment of a dense hybrid wireless sensing system for bridge assessment", *Struct. Infrastruct. E.*, **7**(5), 369-378.
- Gonzalez, A., O'Brien, E.J. and McGetrick, P.J. (2012), "Identification of damping in a bridge using a moving instrumented vehicle", *J. Sound Vib.*, **331**(18), 4115-4131.
- Ihsan, S.I., Ahmadian, M., Faris, W.F. and Blancard, E.D. (2009), "Ride performance analysis of half-car model for semi-active system using RMS as performance criteria", *Shock Vib.*, **16**(6), 593-605.
- Kawamoto, M., Matuoka, K. and Oya, M. (1997), "Blind separation of sources using temporal correlation of the observed signals", *IEICE Trans. Fundamentals*, **E80-A**(4), 695-704.
- Kawatani, M., Kobayashi, Y. and Takamori, K. (1997), "Nonstationary random analysis with coupling vibration of bending and torsion of simple girder bridge under moving vehicles", *J. Struct. Earthq. Eng. - JSCE*, **570/I-40**, 231-238.
- Kim, C.W. and Kawatani, M. (2008), "Pseudo-static approach for damage identification based on coupling vibration with a moving vehicle", *Struct. Infrastruct. E.*, **4**(5), 371-379.
- Lin, C.W. and Yang, Y.B. (2005), "Use of a passing vehicle to scan the fundamental bridge frequencies: an experimental verification", *Eng. Struct.*, **27**(13), 1865-1878.
- McGetrick, P.J., Gonzalez, A. and O'Brien, E.J. (2009), "Theoretical investigation of the use of a moving vehicle to identify bridge dynamic parameters", *Insgiht*, **51**(8), 433-436.

- Nguyen, K.V. and Tran, H.T. (2010), "Multi-cracks detection of a beam-like structure based on the on-vehicle vibration signal and wavelet analysis", *J. Sound Vib.*, **329**(21), 4455-4465.
- Okabayashi, T. (1979), "Mean square response analysis of highway bridges under a single moving vehicle", *Proceedings of the Japan Society of Civil Engineers*.
- Pyzara, A., Bylina, B. and Bylina, J. (2011), "The influence of a matrix condition number on iterative methods' convergence", *Proceedings of the Federated Conference on Computer Science and Information Systems*.
- Ratcliffe, C.P. (1997), "Damage detection using a modified Laplacian operator on mode shape data", *J. Sound Vib.*, **204**(3), 505-517.
- Salawu, O.S. and Williams, C. (1995), "Review of full-scale dynamic testing of bridge structures", *Eng. Struct.*, **17**(2), 113-121.
- Salawu, O.S. (1997), "Detection of structural damage through changes in frequency: a review", *Eng. Struct.*, **19**(9), 718-723.
- Siringoringo, D.M. and Fujino, Y. (2012), "Estimating bridge fundamental frequency from vibration response of instrumented passing vehicle: analytical and experimental study", *Adv. Struct. Eng.*, **15**(3), 443-459.
- Yang, Y.B., Lin, C.W. and Yau, J.D. (2004), "Extracting bridge frequency from the dynamic response of a passing vehicle", *J. Sound Vib.*, **272**(3-5), 471-493.
- Yang, Y.B. and Lin, C.W. (2005), "Vehicle-bridge interaction dynamics and potential applications", *J. Sound Vib.*, **284**(1-2), 205-226.
- Yang, Y.B. and Chang, K.C. (2009a), "Extraction of bridge frequencies from the dynamic response of a passing vehicle enhanced by EMD technique", *J. Sound Vib.*, **322**(4-5), 18-19.
- Yang, Y.B. and Chang, K.C. (2009b), "Extracting the bridge frequencies indirectly from a passing vehicle: parametric study", *Eng. Struct.*, **31**(10), 2448-2459.
- Yin, S.H. and Tang, C.Y. (2011), "Identifying cable tension loss and deck damage in a cable-stayed bridge using moving vehicle", *J. Vib. Acoust.*, **133**(2), 021007.
- Yong, X., Hong, H., James, M.W.B. and Xia, P.Q. (2002), "Damage identification of structures with uncertain frequency and mode shape data", *Earthq. Eng. Struct. D.*, **31**(5), 1053-1066.
- Zang, Y., Wang, L. and Xiang, Z. (2012), "Damage detection by mode shape squares extracted from a passing vehicle", *J. Sound Vib.*, **331**(2), 291-307.
- Zhang, Y., Lie, S.T. and Xiang, Z. (2013), "Damage detection method based on operating deflection shape curvature extracted from dynamic response of a passing vehicle", *Mech. Syst. Signal Pr.*, **35**(1-2), 238-254.

## Notations

$a_{sl}$	Coefficients of interpolation with base function $N_s(x)$ for mode shape $\phi_l(x)$
$F(\mathbf{x}, \mathbf{y})$	The degree of correlations of $\mathbf{x}(= x_1, \dots, x_n)$ and $\mathbf{y}(= y_1, \dots, y_n)$
$L_1 L_2$	Distance of axles from the centroid of a vehicle
$L$	The length of a bridge
$m$	The total number of data for analysis ( $=b - a + 1$ )
$m_e$	Maximum degree of assumed modes in the modal superposition
$m_s$	Mass of heavy vehicle (two axles)
$n_{ve}$	Number of vehicle
$n_t$	The maximum number of time index
$n_{mov}$	The number of moving observation points of $\Delta\tilde{y}_i(t_k)$
$n_d$	The maximum degree of assumed modes
$n_{fix}$	The maximum number of the fixed observation points
$n_x$	Number of contact force
$n_e$	Number of beam element
$N_s(x)$	Base function
$\overline{\text{MAC}}$	The averaged max value
$p_l$	Generalized coordinate for $l$ th shear mode
$P_i(t)$	Contact force of $i$ th axle
$q_l(t)$	The generalized coordinate of the $l$ th vibration mode
$\tilde{r}_i(t_k)$	The road roughness at $\tilde{x}_i(t_k)$
$r(x)$	The roughness at position $x$
$t$	Time
$t_a$	The time when the last vehicle reaches $\hat{x}_1 (= a\Delta t)$
$t_b$	The time when the second vehicle reaches $\hat{x}_{n_{fix}} (= b\Delta t)$
$t_0$	The time when vehicle $i$ enters the bridge
$t_{nL}$	The time when vehicle $i$ leaves the bridge
$t_l$	The time of interest when the vehicle $i$ is on the bridge
$t_{l+\tau}$	The time when the vehicle $i+1$ is on the location where the vehicle $i$ was at the time of $t_l$
$t_k$	Discrete time ( $=k\Delta t$ )
$u_i(t_k)$	Forced displacement of vehicle $i$ at $t = t_k$
$x$	Position
$\hat{x}_j$	The location of the fixed observation points
$\tilde{x}_i(t_k)$	The location of vehicle $i$ at the time of $t_k$
$y(x, t)$	The bridge displacement at position $x$ and time $t$
$\Delta\tilde{y}_i(t_l)$	The difference of bridge displacement between the times of $t_l$ and $t_{l+\tau}$ at $x = \tilde{x}_i(t_l)$
$\Delta\hat{y}_i(t_k)$	The differences of bridge deformation between the times of $t_k$ and $t_{k+\tau}$ at the fixed position $\hat{x}_j$
$\tilde{y}_i(t_k)$	The bridge deformation at $\tilde{x}_i(t_k)$
$z_i(t_k)$	The vertical displacement of the vehicle

$\alpha \Omega \eta \xi$	Parameters for roughness spectrum
$\kappa(\mathbf{A})$	The condition number of matrix $\mathbf{A}$
$\sigma_{\max}(\mathbf{A})\sigma_{\min}(\mathbf{A})$	The maximum and minimum of the singular value of $\mathbf{A}$ ,
$\delta_i(t_k)$	Relative displacement of vehicle $i$ at $t = t_k$
$\phi_l(x)$	The shape function of the $l$ th vibration mode
$\gamma_s(x, t)$	Shear rotation of a beam at position $x$ and time $t$
$v_l$	Shape function for $l$ th shear mode
$\tau$	Time difference between adjacent two vehicles
$\mathbf{C}_V$	The damping matrix of the vehicles
$\mathbf{D}$	Matrix of the difference of bridge displacement in terms of fixed observation points
$\mathbf{g}$	Gravity vector
$\mathbf{K}_V$	The stiffness matrix of the vehicles
$\mathbf{L}(t)$	The transformation matrix
$\mathbf{N}(t_k)$	Matrix of base function
$\mathbf{M}_V$	The mass matrix of the vehicles
$\mathbf{M}_P$	a mass matrix of vehicles for contact force
$\mathbf{P}(t)$	Vector of contact force with a component $P_i(t)$ in the $i$ th row
$\mathbf{q}(t)$	The general coordinates vector for FE analysis
$\Delta \mathbf{q}(t_k)$	The difference of generalized coordinates
$\Delta \bar{\mathbf{q}}(t_k)$	Pseudo general coordinates composing the matrix $\Delta \bar{\mathbf{Q}}$
$\Delta \mathbf{Q}$	Matrix with a component $\Delta \mathbf{q}(t_k)$ in the $k$ th column
$\Delta \bar{\mathbf{Q}}$	Matrix obtained by multiplying $\mathbf{V}_R$ , $\Sigma_R$ and $\mathbf{S}$
$\mathbf{S}$	The orthogonal matrix with the maximum values of each column of $\mathbf{U}$
$\mathbf{u}(t)$	Vector of forced displacements to the vehicles for FE analysis
$\mathbf{UV}$	Orthogonal matrices of singular value decomposition of $\mathbf{D}$
$\mathbf{V}_R$	The matrix consisting of $n_d$ columns of $\mathbf{V}$
$\Delta \hat{\mathbf{y}}(t_k)$	Vector of with a component $\Delta \hat{y}_i(t_k)$ in the $i$ th row
$\mathbf{y}(t)$	The bridge displacement vector for FE analysis
$\mathbf{X}$	The mode shape matrix with a component $\phi_j(x_i)$ in the $i$ th row and $j$ th column
$\mathbf{z}(t)$	Vector of vehicle responses for FE analysis
$\ddot{\mathbf{z}}(t)$	Vector of acceleration responses of the vehicles for FE analysis
$\Phi(t_k)$	Matrix of mode shape
$\bar{\Phi}$	Normalized matrix of $\mathbf{U}$
$\hat{\Phi}$	Matrix with a component $\phi_j(\hat{x}_i)$ in the $i$ th row and $j$ th column
$\Sigma$	The matrix having singular values of $\mathbf{D}$
$\Sigma_R$	Matrix comprising $n_d$ columns of $\Sigma$
$\mathbf{M}_X \mathbf{C}_X \mathbf{K}_X$	Normalized modal mass, damping, and stiffness matrix, respectively
$\mathbf{M}_B \mathbf{C}_B \mathbf{K}_B$	Diagonal matrices with the components $M_i$ , $C_i$ , and $K_i$ at the $i$ th element, respectively